Variability in air-sea O2 and CO2 fluxes and its impact on atmospheric potential oxygen (APO) and the partitioning of land and ocean carbon sinks

C. D. Nevison, N. M. Mahowald, S. C. Doney, I. D. Lima

Biogeosciences Discuss., 4, 2877–2914, 2007
www.biogeosciences-discuss.net/4/2877/2007/

Biogeosciences Discussions

Biogeosciences Discussions is the access reviewed discussion forum of *Biogeosciences*

Variability in air-sea O_2 and CO_2 fluxes and its impact on atmospheric potential oxygen (APO) and the partitioning of land and ocean carbon sinks

C. D. Nevison[1], N. M. Mahowald[1], S. C. Doney[2], and I. D. Lima[2]

[1]National Center for Atmospheric Research, Boulder, Colorado, USA
[2]Dept. of Marine Chemistry and Geochemistry, Woods Hole Oceanographic Institution, Woods Hole, MA, USA

Received: 4 July 2007 – Accepted: 13 July 2007 – Published: 27 August 2007

Correspondence to: C. D. Nevison (nevison@ucar.edu)

Abstract

A three dimensional, time-evolving field of atmospheric potential oxygen (APO ~ O_2/N_2 + CO_2) is estimated using surface O_2, N_2 and CO_2 fluxes from the WHOI ocean ecosystem model to force the MATCH atmospheric transport model. Land and fossil carbon fluxes are also run in MATCH and translated into O_2 tracers using assumed O_2:CO_2 stoichiometries. The model seasonal cycles in APO agree well with the observed cycles at 13 global monitoring stations, with agreement helped by the inclusion of oceanic CO_2 in the APO calculation. The model latitudinal gradient in APO is strongly influenced by seasonal rectifier effects in atmospheric transport, which appear at least partly unrealistic based on comparison to observations. An analysis of the APO vs. CO_2 method for partitioning land and ocean carbon sinks is performed in the controlled context of the MATCH simulation, in which the true surface carbon and oxygen fluxes are known exactly. This analysis suggests uncertainty ranging up to ±0.2 PgC in the inferred sinks due to transport-induced variability. It also shows that interannual variability in oceanic O_2 fluxes can cause increasingly large error in the sink partitioning when the method is applied over increasingly short timescales. However, when decadal or longer averages are used, the variability in the oceanic O_2 flux is relatively small, allowing carbon sinks to be partitioned to within a standard deviation of 0.1 Pg C/yr of the true values, provided one has an accurate estimate of long-term mean O_2 outgassing.

1 Introduction

Atmospheric O_2/N_2 measurements provide complementary information about atmospheric CO_2 due to the close coupling between oxygen and carbon fluxes during fossil fuel combustion and terrestrial photosynthesis/respiration (Keeling et al., 1993). In contrast, oceanic O_2 and CO_2 fluxes are more or less decoupled, for reasons described below. The tracer atmospheric potential oxygen (APO) exploits these differences to

BGD

4, 2877–2914, 2007

remove the terrestrial contribution to changes in atmospheric O_2/N_2, thus allowing the oceanic contribution to be largely isolated. APO is defined as,

$$APO = O_2/N_2 + \frac{1.1}{X_{O2}} CO_2, \quad (1)$$

where 1.1 derives from the approximate – O_2:CO_2 molar ratio of terrestrial photosynthesis/respiration (Severinghaus, 1995; Stephens et al., 1998; Keeling et al., 1998). The parameter X_{O2}=0.2098 is the mole fraction of O_2 in dry air and converts from ppm O_2 to per meg, the units used for O_2/N_2 (Keeling and Shertz, 1992). Fossil fuel combustion, which has a slightly larger –O_2:CO_2 molar ratio of ~1.4, exerts a small influence on APO, although this is reduced by ~80% relative to the original influence on O_2/N_2.

APO data have been used in at least three important carbon cycle applications. First, the seasonal cycle in APO reflects seasonal imbalances between photosynthetic new production in the surface ocean, which occurs largely in spring/summer, and the wintertime ventilation of deeper waters depleted in O_2 due to remineralization. The amplitude of the seasonal cycle in APO has been used to infer the rate of seasonal new production at the ocean basin or hemispheric scale (Bender et al., 1996; Balkanski et al., 1999; Najjar and Keeling, 2000), although uncertainties in the inferred rates arise due to temporal and spatial overlap between new production and ventilation (Nevison et al., 2005; Jin et al., 2007).

Second, the latitudinal gradient in APO in principle reflects global-scale patterns of ocean biogeochemistry and ocean circulation, with O_2 uptake occurring primarily at high latitudes and outgassing of both O_2 and CO_2 taking place in the tropics. The ocean-induced patterns are superimposed on the overall north-to-south increase in APO due to northern hemisphere-dominated fossil fuel combustion. Early atmospheric transport model simulations of the latitudinal gradient in APO resulting from fossil fuel and ocean carbon model fluxes found a mismatch with observations, and suggested that deficiencies in the physical components of the ocean models might be the cause

(Stephens et al., 1998). Later studies suggested that the discrepancies might be attributed mainly to the atmospheric transport models (Gruber et al., 2001; Naegler et al., 2007). A further complication is that the observed APO gradient appears to be evolving with time and displays significant interannual variability (Battle et al., 2006; Hamme et al., 2006).

A third, critically important application of APO data is to constrain the partitioning of anthropogenic CO_2 uptake between the ocean and the land biosphere, which together have absorbed more than half of the anthropogenic carbon put in the atmosphere over the last half century (Battle et al., 2000; Bender et al., 2005; Manning and Keeling, 2006, referred to hereafter as MK06). This application involves solving a system of two equations in two unknowns, as derived from the mass balances for CO_2 and O_2/N_2.

$$\Delta CO_2/\Delta t = \beta(F_{fuel} - F_{land} - F_{ocean}) \quad (2)$$

$$\Delta(O_2/N_2)/\Delta t = \beta\gamma(-\alpha_f F_{fuel} + \alpha_{bio} F_{land}) + Z_{eff}, \quad (3)$$

where β=0.471 is the conversion from Pg C to ppm CO_2, $\gamma = 1/X_{O2}$ is the ppm to per meg conversion factor described above, Z_{eff} is an oceanic O_2 outgassing term in per meg units, and α_{bio}=1.1 and α_f=1.4 are the $-O_2$:CO_2 molar ratios of terrestrial respiration/ photosynthesis and fossil fuel combustion. F_{fuel} is the release of fossil carbon to the atmosphere, which is known from industry data (Marland et al., 2002), while F_{land} and F_{ocean}, the two unknowns, are CO_2 uptake by land and ocean, defined here as positive when they act as sinks for atmospheric CO_2. Equations (2) and (3) can be combined according to the definition of APO in Eq. (1) to yield the APO time derivative:

$$\Delta(APO)/\Delta t = \beta\gamma((\alpha_{bio} - \alpha_f)F_{fuel} - \beta\gamma\alpha_{bio}F_{ocean}) + Z_{eff} \quad (4)$$

One can solve for F_{land} and F_{ocean} using either the system of Eq. (2) and (3) or (2) and (4) based on the global rates of change of CO_2 and O_2/N_2 or CO_2 and APO, respectively, observed by global atmospheric monitoring networks.

The above method, originally presented as a vector diagram (Keeling et al., 1996), assumes that the O_2:CO_2 stoichiometries of fossil fuel combustion and terrestrial respiration/photosynthesis are known, but that oceanic O_2 and CO_2 fluxes are decoupled. The vector method is often considered the best way to monitor the partitioning of sinks for anthropogenic CO_2 on a continuing basis, allowing the detection of trends or changes, e.g., the increased land sink of the 1990s relative to the 1980s (Prentice et al., 2001). The ability to monitor these changes is essential to accurately predicting future levels of CO_2. Alternative methods for estimating ocean and/or land sinks are generally more difficult to update quickly. Ocean inventory methods, for example, require a large new set of ocean cruise data (e.g., Matsumoto and Gruber, 2005).

Despite the advantages of the APO vs. CO_2 method, its inherent uncertainties may be so large that it cannot constrain the carbon sink partitioning to within better than ~±0.7 PgC/yr (LeQuere et al., 2003). This uncertainty represents a substantial fraction of the mean total land and ocean sinks, which are estimated at 1.9 and 1.2 PgC/yr, respectively, for 1990–2000 (*MK*06). Among the inherent uncertainties in the method are those associated with fossil fuel combustion inventories and the assumed -O_2:CO_2 stoichiometries of combustion and terrestrial photosynthesis/respiration. The single largest uncertainty for estimating the ocean carbon sink is the Z_{eff} term associated with oceanic O_2 fluxes (*MK*06).

Early applications of the vector method assumed that the atmosphere-ocean system for O_2 was still essentially in equilibrium and thus that the net annual mean air-sea flux of O_2 was approximately zero (Keeling et al., 1993, 1996). This assumption was closely related to the reasons for the decoupling of oceanic O_2 and CO_2 fluxes. O_2 is far less soluble than CO_2, with only 1% of the O_2 in the ocean-atmosphere system partitioning into the ocean compared to 98% for CO_2. Compounding the solubility difference is the fact that fossil fuel combustion and deforestation have raised atmospheric CO_2 significantly, by ~35% relative to preindustrial levels, thus providing the geochemical driving force for net global oceanic CO_2 uptake. In contrast, these processes have reduced atmospheric O_2/N_2 by only ~240 per meg, or less than 0.03% of the total O_2 burden,

since atmospheric monitoring of O_2/N_2 began in the late 1980s (*MK*06). An additional cause of the decoupling between oceanic O_2 and CO_2 fluxes is the buffering effect of carbonate chemistry in seawater, which increases the air-sea CO_2 equilibration time scale by an order of magnitude relative to that of O_2.

Although the assumption of a net zero annual oceanic O_2 flux initially seemed reasonable, it has long been known that natural interannual variability in oceanic O_2 fluxes, due, e.g., to incomplete ventilation of O_2-depleted thermocline waters in some years, followed by deep convection events in subsequent years, can create a non-zero net oceanic O_2 flux over a given year or even period of years (Keeling et al., 1993). Thus the vector method is generally applied to longer, e.g., decadal averages, of APO and CO_2 data with the assumption that the interannual variability will average to zero. In addition to natural interannual variability, recent studies have recognized that long-term ocean warming may be inducing net O_2 outgassing, with reinforcing feedbacks associated with biology and ocean stratification (Sarmiento et al., 1998; Bopp et al., 2002; Plattner et al., 2002). Both natural interannual variability and long-term net O_2 outgassing are quantified based on empirical relationships between dissolved O_2 and potential temperature extrapolated to observed heat fluxes, although these relationships are not well understood (Keeling and Garcia, 2002). *MK06* estimate the combined effects of these two processes on uncertainty in ocean and land carbon sink partitioning at ±0.5 Pg C/yr.

Here we present a model-based analysis of atmospheric APO and CO_2 focusing on interannual variability in oceanic O_2 fluxes and their contribution to uncertainty in the APO vs. CO_2 method for partitioning carbon sinks. To estimate oceanic O_2, N_2 and CO_2 fluxes, we employ a process-based ocean ecosystem/general circulation model, which represents an advance over the OCMIP-based ocean carbon models that were used predominantly in previous APO studies (Stephens et al., 1998; Naegler et al., 2007). The ocean fluxes are used to force atmospheric transport model simulations that include full interannual variability in the meteorological drivers. We also run fossil and terrestrial CO_2 fluxes, which can be scaled to O_2 based on assumed stoichiome-

tries, in the transport model. Our simulation encompasses a complete set of atmospheric tracers that can be used to evaluate uncertainties in the APO vs. CO_2 method in a controlled model context in which the true surface CO_2 and O_2 fluxes are known exactly. We begin in Sect. 2 with a description of the atmospheric tracer transport model and ocean, land and fossil fuel fluxes, as well as the APO observations used to evaluate model results. We present a comparison of model vs. observed seasonal cycles and latitudinal gradients in Sects. 3.1 and 3.2, respectively. In Sect. 3.3 we characterize the interannual variability in model APO and in Sect. 3.4 we analyze the impact of interannual variability in oceanic O_2 fluxes on the APO vs. CO_2 method for partitioning carbon sinks. This section also effectively includes an analysis of the impact of transport-induced variability on the method, which ordinarily was not reported as one of its uncertainties. We conclude with a summary of our results in Sect. 4.

2 Methods

2.1 Atmospheric Transport Model

The Model of Atmospheric Transport and Chemistry (MATCH) (Rasch et al., 1997; Mahowald et al., 1997) was used to simulate the atmospheric distribution of a range of surface O_2, CO_2 and N_2 fluxes. The model is run at T62 horizontal resolution (about 1.9° latitude by longitude) with 28 vertical levels and a time step of 20 min using archived 6 hourly winds for the years 1979–2004 from the National Center for Environmental Prediction (NCEP) reanalyses (Kalnay et al., 1996). The surface fluxes used to force the simulations are outlined below. See also Nevison et al. (2007)[1] for additional details.

[1] Nevison, C. D., Mahowald, N. M., Doney, S. C., Lima, I. D., van der Werf, G. R., Randerson, J. T., Baker, D. F., Kasibhatla, P., and McKinley, G. A.: Contribution of ocean, fossil fuel, land biosphere and biomass burning carbon fluxes to seasonal and interannual variability in atmospheric CO_2, J. Geophys. Res., submitted, 2007.

2.2 Oceanic O_2, CO_2 and N_2 fluxes

Oceanic O_2 and CO_2 fluxes were obtained for 1979–2004 from the WHOI-NCAR-UC Irvine ocean general circulation model/marine ecosystem model (abbreviated here as the WHOI model). The ecosystem model includes a nutrient-phytoplankton-zooplankton-detritus (NPZD) food web with multi-nutrient limitation (N, P, Si, Fe) and specific phytoplankton functional groups (Doney et al., 1996; Moore et al., 2002, 2004). The general circulation model is the Parallel Ocean Program (POP), which was run at 3.6° longitude resolution and variable latitude resolution ranging from 0.6° near the equator to 2.8° at mid-latitudes, and forced with daily-averaged NCEP reanalysis surface wind, heat flux, atmospheric temperature and humidity, and satellite data products from 1979–2004 (Doney et al., 1998, 2007).

While O_2 and CO_2 fluxes were obtained prognostically from the WHOI model, N_2 fluxes were diagnosed based on the NCEP heat fluxes (Q) as $F_{N2}=Q(dS_{N2}/dT)/C_p$ (Keeling et al., 1998), where dS_{N2}/dT is the temperature derivative of N_2 solubility evaluated at the NCEP sea surface temperature. A similar equation was used to estimate the thermal component of the WHOI O_2 flux: $F_{O2\_thermal}=Q(dS_{O2}/dT)/C_{p,}$, but with two modifications based on the model study of Jin et al. (2007). First, the magnitude of $F_{O2\_thermal}$ was scaled down by a factor of 0.7. Second, the flux was delayed for half a month to account for non-instantaneous air-sea equilibration. Similar modifications were not applied to F_{N2} since their appropriateness for N_2 has not yet been evaluated (X. Jin, personal communication).

In addition to the interannually-varying WHOI and NCEP-based fluxes, MATCH was also run from 1988–2004 with a variety of climatological oceanic CO_2, O_2, and N_2 fluxes. These included the monthly sea surface CO_2 flux climatology of Takahashi et al. (2002) (corrected to 10 m height windspeeds) and the monthly O_2 and N_2 flux anomaly climatology of Garcia and Keeling (2001) (hereafter referred to as GK01). The *GK01* O_2 fluxes are based on linear regressions that use ECMWF heat flux anomalies to spatially and temporally extrapolate historical dissolved O_2 data. These empirical re-

gressions reflect both biology/circulation and thermal-driven variations in oxygen flux. The N_2 flux anomalies are calculated from the same formula for F_{N2} above, but use climatological ECMWF values rather than interannually-varying NCEP data for Q. The monthly O_2 and N_2 flux anomalies have an annual mean of zero at all gridpoints and thus do not provide realistic spatial distributions. To fill this gap, additional simulations were performed with O_2 and N_2 fluxes from the annual mean ocean inversions of Gruber et al. (2001) and Gloor et al. (2001). The inversions are based on ocean inventory data and are subject to ocean general circulation model biases but independent of atmospheric transport influences.

2.3 Fossil fuel and land biosphere carbon fluxes

Fossil fuel carbon emissions, including a small contribution from cement manufacture, were constructed from decadal 1°×1° maps (Andres et al., 1996; Brenkert, 1998) that were interpolated between decades based on the annual regional totals of (Marland et al., 2003). The carbon fluxes were run in MATCH from 1979–2004. The atmospheric O_2 distributions resulting from fossil fuel combustion were estimated from MATCH CO_2 multiplied by a mean fossil fuel O_2:CO_2 stoichiometry of –1.4 (*MK*06).

Two versions of the CASA land biosphere model were used for terrestrial CO_2 fluxes. The first was a cyclostationary (i.e., the same seasonal cycle repeated every year) "neutral biosphere" (NB) version, run in MATCH from 1979–2004, in which annual net ecosystem production (NEP) was assumed to be zero at each grid cell (Olsen and Randerson, 2004). The second was the Global Fire Emissions Database (GFED v2) version of CASA, which incorporates satellite-based estimates of burned area (Randerson et al., 2005; Van der Werf et al., 2006) and for which the biomass burning component of the emissions was optimized based on CO inversion results (P. Kasibhatla, personal communication, 2006). The GFED fluxes provide more realistic interannual variability in atmospheric CO_2 than the NB fluxes, but are limited to 1997–2004 (Nevison et al., 2007[1]). At their original 1°×1° resolution, the global mean GFED carbon flux was constrained to equal zero over the 1997–2004 period, and the NB fluxes had

an annual mean of zero every year. However, a small interpolation error in converting to the T62 MATCH grid resulted in a small net source of CO_2 to the atmosphere of ~+0.1 PgC/yr for both versions of the land flux over these respective periods.

2.4 Model APO

Model atmospheric potential oxygen (APO) was calculated somewhat differently than observed APO (Eq. 1), since O_2 and N_2 were run as separate tracers in MATCH. We used Eq. (5), in which all individual O_2, N_2 and CO_2 tracers are in ppm of dry air and APO is in per meg units (Stephens et al., 1998; Naegler et al., 2007).

$$\mathrm{APO} = \frac{1}{\mathrm{XO2}}(\mathrm{O}_2^{oc} - 1.4\mathrm{CO}_2^{FF}) - \frac{1}{\mathrm{XN2}}\mathrm{N}_2^{oc} + \frac{1.1}{\mathrm{XO2}}(\mathrm{CO}_2^{oc} + \mathrm{CO}_2^{FF}). \quad (5)$$

where the superscripts oc and FF denote ocean and fossil fuel tracers, respectively. X_{O2} and X_{N2} are the fractions of O_2 and N_2 in air (0.20946 and 0.78084, respectively). Land O_2 and CO_2 tracers could have been included in the first and third right hand side terms of Eq. (1), respectively, but simply would have canceled out, since we assumed that O_2^{land}=–1.1 CO_2^{land}. In practice, the CO_2^{FF} terms were important for latitudinal gradients, but had little effect on seasonal or interannual variability. For some applications, the fossil terms were omitted to yield a quantity we refer to as APO^{oc}, which includes only the oceanic tracers. To examine the consequences of neglecting CO_2^{oc} in calculating APO^{oc}, a third quantity, referred to here as O_2/N_2^{oc}, was computed:

$$\mathrm{O}_2/\mathrm{N}_2^{oc} = \frac{1}{\mathrm{XO2}}\mathrm{O}_2^{oc} - \frac{1}{\mathrm{XN2}}\mathrm{N}_2^{oc}. \quad (6)$$

2.5 Observed APO

For comparison to model results, we used observed seasonal cycles from Battle et al. (2006), who computed the 1996-2003 climatological cycles at 13 land-based atmospheric monitoring stations, including both the SIO (Keeling et al., 1998) and Princeton

(Bender et al., 2005) networks. Battle et al. (2005) also determined the latitudinal gradient in APO from the annual mean offsets of sinusoidal fits to the observed seasonal cycles at the land-based monitoring stations and from additional ship-based measurements in the Pacific Ocean.

3 Results and discussion

3.1 Seasonal cycles

The seasonal cycles in APO predicted by the WHOI/MATCH simulation generally agree well with the observed climatological seasonal cycles (Figs. 1–2). The model amplitude is captured to within ±10 to 20% at most stations and the agreement in phasing is excellent at all stations, except PSA, where the model minimum is a month earlier than observed. Oceanic CO_2, although sometimes neglected when calculating the APO seasonal cycle, appears to contribute in a small but non-negligible manner to the amplitude agreement at many stations. Neglecting CO_2^{oc} leads to a greater underestimate of the seasonal amplitude at the tropical SMO and KUM stations, where the CO_2^{oc} and O_2 seasonal cycles are in phase, and a tendency to overestimate the seasonal amplitude at extratropical southern stations, where CO_2^{oc} opposes O_2. In comparison to the WHOI seasonal cycles, the MATCH simulation with climatological O_2, N_2 and CO_2^{oc} fluxes (*GK*01; Takahashi et al., 2002) yields seasonal cycles in APO that agree more poorly in phasing with observations, and tend to overestimate the observed amplitude by 30-40% at most extratropical stations.

WHOI model results suggest that net total oceanic O_2 fluxes do not always correlate well with thermal O_2 or heat fluxes (Fig. 1), as is assumed by the *GK01* seasonal O_2 climatology. At southern extratropical stations in particular, thermal O_2 fluxes are only moderately well correlated in shape and phasing (R=0.4–0.9) and only account for 10–15% of the amplitude of net O_2 seasonal cycle. At tropical and northern stations, the thermal O_2 flux tends to correlate better and account for a larger (20–40%) share of

the seasonal amplitude. These results suggest spatial heterogeneity among different ocean regions in the correlation between thermal O_2 fluxes and fluxes associated with reinforcing effects from biology and ocean circulation. Figures 1–2 suggest that the explicit modeling of ocean biology and circulation provided by the WHOI model can yield superior results to the climatology. Similarly, the more sophisticated ocean ecosystem dynamics of the WHOI model appears to yield more realistic seasonal cycles in APO than the P-restoring OCMIP ocean biology parameterizations tested by Naegler et al. (2007).

A caveat on the above discussion is that previous studies have found that the choice of atmospheric transport model can influence the amplitude of the model seasonal cycle in APO, although it does not tend to alter the phasing of the cycle (Battle et al., 2006; Naegler et al., 2007). These studies found that strong seasonal rectifiers like TM3 tend to yield larger seasonal amplitudes than weak rectifiers like TM2. Naegler et al. (2007) assumed that the average of simulations with TM2 and TM3 was the best estimate of true APO, but Battle et al. (2006) suggested that TM3 may overestimate tracer concentrations and thus seasonal amplitudes due to excessive vertical trapping in surface layers. Transport model differences may explain the discrepancy between the results of GK01 with TM2, which capture the amplitude of the observed APO cycle to within ±10%, albeit with some phasing errors, and those shown here in Fig. 2c, in which the GK01 climatology/MATCH simulation tends to overestimate the observed APO seasonal cycle by 30–40%. Uncertainties associated with atmospheric transport are discussed further below in the context of latitudinal gradients.

3.2 Latitudinal gradient

MATCH predicts non-zero annual mean values of APO^{oc}, when forced with the GK01 O_2 and N_2 seasonal flux anomalies (which are zero at all gridpoints in the annual mean) and the Takahashi et al. (2002) CO_2 fluxes. Positive values of up to ~20 per meg are predicted over northern ocean regions centered around 45–60° N and up to ~10 per meg at comparable southern latitudes (Fig. 3a). Similar but weaker patterns appear in

simulations with the seasonally varying WHOI fluxes (Fig. 3b). In contrast, the annual mean O_2 climatology simulation (Fig. 3c) yields negative annual mean values of APO^{oc} over the mid to high latitude oceans, consistent with the known patterns of net oceanic O_2 uptake in these regions. We also constructed a "composite" annual/seasonal climatology, as per Gruber et al. (2001) and Battle et al. (2006), by adding the results of MATCH simulations with the annual climatology and the GK01 seasonal anomalies. The composite climatology yields an APO^{oc} field similar to that of the WHOI model (Fig. 3d). The results shown in Fig. 3 suggest that the MATCH transport model introduces a seasonal rectifier influence for simulations that include a seasonally varying oceanic O_2 flux component.

The MATCH rectifier effect is caused by at least two interrelated mechanisms. First, the MATCH planetary boundary layer is shallower in summer over the ocean than in winter, due to increased convective heat release in wintertime (Fig. 4). Since positive O_2 flux anomalies occur during summer at mid-high latitudes, they are more likely to be trapped near the surface, resulting in a net positive APO anomaly. Stephens et al. (1998) and Gruber et al. (2001) found a similar effect with the TM2 and GCTM transport models. A second, related mechanism also contributes to the MATCH rectifier effect. The sum of convective and large-scale precipitation, which is effectively a proxy for ventilation of surface layers by upward motion associated with storms, displays strong seasonal and hemispheric differences (Fig. 4). More storms occur over the ocean in the northern vs. the southern hemisphere and more storms occur in winter vs. summer in both hemispheres. Thus, negative winter O_2 fluxes are more likely to be ventilated from the boundary layer, especially in the northern hemisphere, helping to explain the winter/summer pattern in both hemispheres as well as the stronger seasonal difference in the north.

The "APO Transcom" intercomparison showed that the majority of 9 transport models tested, using the GK01 seasonal anomalies to produce the quantity referred to in this study as O_2/N_2^{oc}, yielded similar rectifier effects to those described above (Blaine, 2005). MATCH:NCEP fell among the strong rectifiers, but produced weaker annual

mean values than some of the other transport models in that class. TM2 fell among the weak rectifiers, especially when forced with the 1986 ECMWF winds used by GK01. All 9 models produced negative annual mean values of O_2/N_2^{oc} in the tropics. That result has been attributed to a preferential influence of the winter hemisphere on the tropics due to ITCZ shifts, since mid to high latitude O_2 fluxes are negative in winter (Stephens et al., 1998). The current MATCH simulations also yield tropical minima in O_2/N_2^{oc} (not shown), but these are mostly canceled in APO^{oc} by the inclusion of CO_2^{oc}, which outgases strongly in the tropics (Fig. 3a).

The MATCH seasonal rectifier effects appear to be at least partly unrealistic based on comparison with observed APO. The "equatorial bulge" in APO, a prominent feature of the observations, is pulled down in WHOI/MATCH results by the strong mid to high latitude O_2 maxima and tropical minima associated with the seasonal rectifier (Figs. 5a, d). In contrast, MATCH runs with the annual mean O_2 flux climatology capture the "equatorial bulge" relatively well (Figs. 5c, f). The composite annual/seasonal climatology yields a rectifier-effect-dominated latitudinal gradient that resembles the WHOI/MATCH results and underestimates the equatorial bulge (Figs. 5b, e). Battle et al. (2006) found similar results for TM3 simulations using the same composite climatology, although they emphasized the improved agreement between the model and observed latitudinal gradient study relative to Stephens et al. (1998). That study found that forward runs of TM2 with surface fluxes from various ocean models produced an equatorial bulge in APO^{oc} that seemed unrealistically large. Collectively, these results suggest that some degree of rectification, somewhere between that predicted by TM2 vs. by TM3 or MATCH, might actually occur in the real world.

Aside from the equatorial bulge, WHOI oceanic CO_2 creates a greater north-to-south increase in APO, due to the natural southward net transport of inorganic carbon in the ocean, than the Takahashi et al. (2002) CO_2 climatology (Nevison et al., 2007[1]), such that WHOI tends to agree better with observed APO (Figs. 5a, b). However, fossil fuel, for which we used the same MATCH tracer in both the WHOI and climatological gradients, also contributes to this north-to-south increase. Otherwise, the APO obser-

vations lack clear patterns and none of the three simulations shown in Fig. 5 matches the observations particularly well. Overall, our results support the conclusion of Naegler et al. (2007), i.e., that evaluating ocean models (or flux climatologies) based on the latitudinal gradient in APO is complicated by uncertainties in atmospheric transport. The interannual variability and complexity of the observations further complicate the evaluation (Battle et al., 2006).

3.3 Interannual variability

Interannual variability in WHOI/MATCH APO has about the same amplitude range (±5 to 10 per meg) as observations (Bender et al., 2005; R. Keeling, personal communication) (Fig. 6). Also consistent with observations is the model's prediction that variability is moderately coherent among monitoring stations within a hemisphere (Fig. 7). For example, the correlation coefficient R for modeled interannual variability at CGO (41° S, 145° E) vs. MQA (54° S, 159° E) is ~0.65, suggesting the presence of common large-scale signals as well as local variability around each station (Hamme et al., 2006). A breakdown of model APO into its components shows that oceanic O_2 fluxes are the main drivers of interannual variability (Figs. 8a, b). CO_2^{oc} also contributes substantially to interannual variability in APO in the tropics, accounting for as much as half of the relatively low total variability predicted there (Fig. 8b).

More generally, most of the interannual variability in WHOI/MATCH APO originates at mid to high latitudes, especially in the Southern Ocean (Fig. 8a). In contrast, (McKinley et al., 2003) found that North Atlantic convection events and tropical ENSO cycles were responsible for most of the variability in their model ocean O_2 fluxes. Part of the difference between the two studies may be due to the incorporation of iron limitation, including interannual variability in iron dust deposition, in the WHOI ocean ecosystem model, which leads to large variability in O_2 fluxes from the Southern Ocean. It is also possible that the underlying POP ocean general circulation model may underestimate deep convection events in the North Atlantic.

In general, interannual variability in WHOI/MATCH total O_2 is moderately correlated

to variability in thermal O_2 (R ~0.6 to 0.8), but the ratio of total:thermal variability is spatially heterogeneous, with highest ratios in the Southern Ocean and lowest ratios in the tropics (Fig. 8c). The underlying total O_2 flux:heat flux ratios of the WHOI model, which drive the patterns in Fig. 8c, range from >10 nmol/J in some seasons in the Southern Ocean to 1–2 nmol/J in the tropics and <0 in the equatorial upwelling zone, where, in contrast to most ocean regions, solubility and biology/circulation act in opposite directions on O_2 (Stephens et al., 1998). These patterns are generally consistent with O_2^*/θ slopes observed in the ocean thermocline (Keeling and Garcia, 2002). Overall, Figs. 6–8 demonstrate that the WHOI/MATCH simulation generally yields a realistic range of variability in APO, despite some shortcomings, and help establish the model as a useful tool for examining the influence of variability in ocean O_2 fluxes on uncertainty in the APO vs. CO_2 method for partitioning carbon sinks.

3.4 Partitioning carbon sinks using APO and CO_2

The MATCH simulation offers a self-contained system for exploring some of the uncertainties in the APO vs. CO_2 method for partitioning land and ocean carbon sinks (presented in the Introduction) in a more controlled manner than is possible in the real world. The model simulation contains no measurement error or drift in $\Delta CO_2/\Delta t$ and $\Delta APO/\Delta t$ and no uncertainties in α_{bio}, α_f, F_{fuel}, or Z_{eff}. In addition, F_{land} and F_{ocean} can be computed exactly by globally integrating the fluxes used to force MATCH. These "true" fluxes can be compared to the F_{land} and F_{ocean} terms inferred by solving Eqs. (2) and (4) using the time derivatives of the MATCH APO and CO_2 tracers (Fig. 9). Having eliminated all conventional sources of uncertainty, the model simulation allows the examination of 1) the uncertainty in the method arising from variability introduced by transport acting on surface fluxes, and 2) the uncertainty arising from the O_2 outgassing term Z_{eff}, which, like the true carbon sinks, can be calculated exactly by globally integrating the oceanic O_2 fluxes used to force MATCH.

Early applications of the vector method solved the O_2/N_2 mass balance (Eq. 3) first for F_{land} and then used that result to solve the CO_2 mass balance (Eq. 2) for F_{ocean}

(Keeling et al., 1996). We have followed the more recent preference for solving the APO mass balance (Eq. 4) first for F_{ocean} and then Eq. (2) for F_{land}. This second approach offers several advantages over the O_2/N_2 vs. CO_2 system, including the ability to use global atmospheric CO_2 datasets from the NOAA/CCGG network to solve Eq. (2) instead of CO_2 data from the more limited number of O_2/N_2 monitoring stations [MK06]. The reader is referred to Bender et al. (2005) and MK06 for more details on solving the APO and CO_2 system of equations.

Figure 10a demonstrates that transport introduces large uncertainties, especially in F_{land}, when individual station data are used to estimate $\Delta CO_2/\Delta t$. This transport uncertainty is reduced when global $\Delta CO_2/\Delta t$ is substituted for the individual station data (Fig. 10b) and is further reduced when $\Delta APO/\Delta t$ is calculated from the average of a group of stations rather than a single station (Fig. 10c). For the particular time span (Δt=1997 to 2004=8 years) shown in Fig. 10c, the average $\Delta APO/\Delta t$ of ALT, LJO and CGO approaches the "true" sinks most closely, but this is not necessarily the case for other time spans. All of the station groupings shown, which were chosen because they have been used in real-life applications, give a good approximation of the truth. We chose the ALT, LJO and CGO combination (favored by MK06) to explore the impact of different time spans and staggered decadal intervals on the APO vs. CO_2 method. In this exercise, we used MATCH simulations with both the CASA GFED tracer (with realistic interannual variability in land CO_2), which was available only from 1997–2004, and the CASA NB tracer, which has unrealistically small variability in land CO_2, but allows the exploration of broader time intervals from 1979–2004. We found that staggered decadal time spans (using the NB land CO_2 tracer) have some scatter associated with transport uncertainty, but give true F_{land} and F_{ocean} to within ±0.2 PgC/yr or better (Fig. 10d) with a standard deviation of only ~0.05 PgC/yr. Similarly, we found that time spans of varied length (Figs. 10e–f) have some scatter due to transport uncertainty, but give the true answer generally to within ±0.2 PgC/yr. The longer time spans tend to approach the truth more closely, and simulations with the GFED land CO_2 tracer tend to produce more scatter than those with the NB land CO_2 tracer (Figs. 10e, f). From

the above results, we conclude that transport influences acting on surface fluxes introduce a small error into the CO_2 land and ocean sinks inferred using the APO vs. CO_2 method of generally less than ±0.2 PgC. This error reflects uncertainty not only in the partitioning between land and ocean sinks, but also in the absolute magnitude of the combined sinks (which is set by $F_{fuel} - \Delta CO_2/\Delta t$), since the transport uncertainty affects $\Delta CO_2/\Delta t$. It is possible that spurious seasonal rectifier effects for both APO, as discussed above, and CO_2 (Denning et al., 1995; Gurney et al., 2003) may bias the model uncertainty on the high side relative to the real world. However, it is difficult to quantify this bias without knowing more quantitatively whether and how the transport effects are "wrong."

In all the results discussed above for Fig. 10, the true Z_{eff} is known exactly and used to solve Eqs. (4) and (2). Figures 10c, 11 and 12 investigate what happens in the more realistic case where the O_2 outgassing term is not exactly known. Figure 10c shows that ignoring O_2 outgassing entirely leads to a clear underestimate of the ocean carbon sink F_{ocean}. This is true whether the CASA NB or GFED land CO_2 tracer is used. The neglect of Z_{eff} leads to a compensating overestimate of the true land sink in the NB case, but ends up partly canceling transport error in F_{land} in the GFED case, such that the true F_{land} is estimated about equally well with or without Z_{eff} (Fig. 10c).

In real-life applications of the APO vs. CO_2 method, O_2 outgassing is not ignored (Battle et al., 2000; Bender et al., 2005; MK06). Rather, current studies have an arguably good estimate of the long-term mean Z_{eff} based on observed ocean heat fluxes and empirical and/or modeled O_2:heat flux or O_2^*:θ ratios (Bopp et al., 2002; Keeling and Garcia, 2002; Plattner et al., 2002). However, the studies still assume that natural interannual variability in oceanic O_2 fluxes averages to zero for the time period (commonly ~1 decade) over which they apply the APO vs. CO_2 method. Figure 11 suggests that this is a reasonable assumption, according to the WHOI model. In Fig. 11a, four different 10-year average O_2 fluxes, calculated at staggered intervals over the 25-year span of the ocean model simulation, deviate relatively little (σ=±6 Tmol O_2/yr) from the long-term 25-year mean of 30 Tmol O_2/yr. This is true despite the relatively large

BGD
4, 2877–2914, 2007

range of interannual variability (–50 to +85 Tmol O_2/yr) in the O_2 fluxes. The model 25-year mean corresponds closely to the value of Z_{eff} used in calculations involving observed APO and CO_2 (Keeling and Garcia, 2002; MK06). When this 25-year mean is substituted for the true 10-year averages in the model APO vs. CO_2 calculations, the resulting estimate of F_{ocean} is only slightly worse than that estimated when the exact Z_{eff} is used, given the small transport-related background error that already exists in the calculation (Fig. 11b).

When one moves to shorter, e.g., 5-year, averages, the above conclusions start to break down. The eight staggered 5-year average O_2 fluxes shown in Fig. 11a deviate more substantially (σ=±16 Tmol O_2/yr) from the 30 Tmol/yr long-term mean than did the 10-year averages. Accordingly, the values of F_{ocean} calculated by substituting the long-term mean Z_{eff} for the true 5-year averages display larger deviations from the truth, with errors of up to ±0.5 Pg C/yr. For even shorter time intervals, e.g., 1-year averages, the problem is compounded further, leading to large errors and unrealistic year-to-year swings in the inferred value of F_{ocean} of ±1 PgC/yr or more, consistent with previous studies (McKinley et al., 2003; Bender et al., 2005).

To quantify more systematically the error involved in applying Eqs. (4) and (2) over a particular time average, we analyzed the standard deviation from the "truth" in F_{ocean} calculated using both the long-term mean Z_{eff} and the true Z_{eff}. The calculations were performed over Δt intervals ranging from 1 to 15 years, in which all whole-year staggered intervals for each respective Δt between 1980 and 2003 were considered. The results of the systematic calculations using true Z_{eff} confirmed the patterns suggested by the more anecdotal calculations in Figs. 10d–f and 11. The standard deviation σ of F_{ocean} from the truth is <0.1 PgC/yr for Δt=15 to ~3 years, with a small increasing trend in σ as Δt decreases (Fig. 12). Intervals of $\Delta t \leq 3$ year show a steeper increase in σ associated with the increased transport uncertainty involved in calculating $\Delta APO/\Delta t$ and, to a lesser extent, global $\Delta CO_2/\Delta t$ over a short time span. Calculations substituting the 1980–2003 mean Z_{eff} for the true Z_{eff} have a somewhat larger σ in F_{ocean} for all time intervals, but σ remains <0.1 PgC/yr for Δt ranging from 15 to ~9 yrs. However,

BGD
4, 2877–2914, 2007

as Δt decreases from 9 to 4 years, σ begins to increase more sharply, paralleling the increasing standard deviation of true Z_{eff} from long-term mean Z_{eff} (Fig. 12). For Δt≤3 years, the increase in σ steepens still more, due to the increased influence of transport uncertainty on ΔAPO/Δt, as discussed above.

4 Conclusions

Atmospheric potential oxygen (APO) can be estimated from atmospheric transport model simulations forced by modeled or climatological oceanic O_2, N_2 and CO_2 fluxes and supporting fossil carbon fluxes. Forward simulations of the MATCH atmospheric transport model, using surface fluxes from the WHOI ocean ecosystem model, appear comparable or superior to climatological ocean fluxes in reproducing observed seasonal and spatial patterns in APO. However, transport uncertainties, especially those associated with a questionable seasonal rectifier effect, weaken these conclusions. Oceanic O_2 fluxes dominate seasonal, spatial and interannual variability in simulated APO, but oceanic CO_2 fluxes can contribute substantially to all 3 types of variability, especially in the tropics. The WHOI model predicts strong interannual variability in the annual mean ocean O_2 flux (range –50 to +85 Tmol O_2/yr), which is concentrated largely at high latitudes and displays a spatially and temporally heterogeneous total:thermal O_2 flux ratio. An analysis of the APO vs. CO_2 method for partitioning land and ocean carbon sinks, performed in the controlled context of the MATCH simulation, in which the true surface carbon and oxygen fluxes are known exactly, suggests a small uncertainty (ranging up to ±0.2 Pg C) in the sinks due to transport-induced variability. Natural interannual variability in ocean O_2 fluxes introduces only a small error into the inferred carbon sink partitioning when the APO vs. CO_2 method is applied over decadal periods, but this error increases substantially when the method is applied over shorter and shorter intervals.

Acknowledgements. We acknowledge the support of NASA grant NNG05GG30G and NSF grant ATM0628472. We also thank M. Battle, H. Garcia, S. Mikaloff Fletcher, R. Keeling,

M. Bender, J. Randerson, G. van der Werf, and P. Kasibhatla for providing APO data and model or climatological fluxes. The MATCH simulations were conducted at the National Center for Atmospheric Research, a National Science Foundation funded facility.

References

Andres, R. J., Marland, G., Fung, I., and Matthews, E.: A 1°×1° distribution of carbon dioxide emissions from fossil fuel consumption and cement manufacture, 1950–1990, Global Biogeochem. Cycles, 10, 419–429, 1996.

Balkanski, Y., Monfray, P., Battle, M., and Heimann, M.: Ocean primary production derived from satellite data: An evaluation with atmospheric oxygen measurements, Global Biogeochem. Cycles, 13, 257–271, 1999.

Battle, M., Bender, M. L., Tans, P. P., White, J. W. C., Ellis, J. T., Conway, T., and Francey, R. J.: Global carbon sinks and their variability inferred from atmospheric and d13C, Science, 287, 2467–2470, 2000.

Battle, M., Mikaloff Fletcher, S., Bender, M. L., Keeling, R. F., et al.: Atmospheric potential oxygen: New observations and their implications for some atmospheric and oceanic models, Global Biogeochem. Cycles, 20, GB1010, doi:10.1029/2005GB002534, 2006.

Bender, M., Ellis, T., Tans, P., Francey, R., and Lowe, D.: Variability in the O_2/N_2 ratio of southern hemisphere air, 1991–1994: Implications for the carbon cycle, Global Biogeochem. Cycles, 10, 9–21, 1996.

Bender, M., Ho, D., Hendricks, M. B., Mika, R., Battle, M. O., Tans, P. Conway, T. J., Sturtevant, B., and Cassar, N.: Atmospheric O_2/N_2 changes, 1993–2002: Implications for the partitioning of fossil fuel CO_2 sequestration, Global Biogeochem. Cycles, 19, 9–21, 2005.

Blaine, T. W.: Continuous Measurements of Atmospheric Ar/N_2 as a Tracer of Air-Sea Heat Flux: Models, Methods, and Data, Ph. D. Thesis, University of California, San Diego, La Jolla, 225 pp., 2005.

Bopp, L., Le Quere, C., Heimann, M., Manning, A. C., and Monfray, P.: Climate-induced oceanic oxygen fluxes: Implications for the contemporary carbon budget, Global Biogeochem. Cycles, 16, GB1022, doi:10.1029/2001GB001445, 2002.

Brenkert, A. L.: Carbon dioxide emission estimates from fossil-fuel burning, hydraulic cement

production, and gas flaring for 1995 on a one degree grid cell basis, available at http://cdiac.esd.ornl.gov/ndps/ndp058a.html, 1998.
Denning, A. S., Fung, I. Y., and Randall, D. A.: Latitudinal gradient of atmospheric CO_2 due to seasonal exchange with land biota, Nature, 376, 240–243, 1995.
Doney, S. C., Glover, D. M., and Najjar, R. G.: A new coupled, one-dimensional biological-physical model for the upper ocean: Applications to the JGOFS Bermuda Atlantic Time-series Study (BATS) site, Deep-Sea Res. Pt. II, 43, 591–624, 1996.
Doney, S. C., Large, W. G., and Bryan, F. O.: Surface ocean fluxes and water-mass transformation rates in the coupled NCAR Climate System Model, J. Climate, 11, 1420–1441, 1998.
Doney, S. C., Yeager, S., Danabasoglu, G., Large, W. G., and McWilliams, J. C.: Mechanisms governing interannual variability of upper ocean temperature in a global hindcast simulation, J. Phys. Oceanogr., 37, 1918–1938, 2007.
Garcia, H. E. and Keeling, R. F.: On the global oxygen anomaly and air-sea flux, J. Geophys. Res., 106, 31 155–31 166, 2001.
Gloor, M., Gruber, N., Hughes, T. M., and Sarmiento, J. L.: An inverse modeling method for estimation of net air-sea fluxes from bulk data: Methodology and application to the heat cycle, Global Biogeochem. Cycles, 15, 767–782, 2001.
Gruber, N., Gloor, M., Fan, S.-M., and Sarmiento, J. L.: Air-sea flux of oxygen estimated from bulk data: Implications for the marine and atmospheric oxygen cycles, Global Biogeochem. Cycles, 15, 783–803, 2001.
Gurney, K. R., Law, R. M., Denning, A. S., Rayner, P. J., et al.: Transcom 3 CO_2 inversion intercomparison: 1. Annual mean control results and sensitivity to transport and prior flux information, Tellus B, 55, 555–579, 2003.
Hamme, R. C., Keeling, R. F., and Paplawsky, W. J.: Explaining observed variability in the interhemispheric gradient of atmospheric potential oxygen, AGU Fall Meeting, San Francisco, USA, 11–15 December 2006, OS52C-03, 2006.
Jin, X., Najjar, R. G., Louanchi, F., and Doney, S. C.: A modeling study of the seasonal oxygen budget of the global ocean, J. Geophys. Res., 112, C05017, doi:10.1029/2006JC003731, 2007.
Kalnay, E., Kanamitsu, M., Kistler, R., Collins, W., Deaven, D., et al.: The NMC/NCAR 40-year reanalysis project, B. Am. Meteorol. Soc., 77, 437–471, 1996.
Keeling, R. F. and Shertz, S. R.: Seasonal and interannual variations in atmospheric oxygen

and implications for the global carbon cycle, Nature, 358, 723–727, 1992.
Keeling, R. F. and Garcia, H. E.: The change in oceanic O_2 inventory associated with recent global warming, P. Natl. Acad. Sci. USA, 99, 7848–7853, 2002.
Keeling, R. F., Najjar, R. P., Bender, M. L., and Tans, P. P.: What atmospheric oxygen measurements can tell us about the global carbon cycle, Global Biogeochem. Cycles, 7, 37–67, 1993.
Keeling, R. F., Piper, S. C., and Heimann, M.: Global and hemispheric CO_2 sinks deduced from changes in atmospheric O_2 concentration, Nature, 391, 218–221, 1996.
Keeling, R. F., Stephens, B. B., Najjar, R. G., Doney, S. C., Archer, D., and Heimann, M.: Seasonal variations in the atmospheric O_2/N_2 ration in relation to the kinetics of air-sea gas exchange, Global Biogeochem. Cycles, 12, 141–163, 1998.
Le Quéré, C., Aumont, O., Bopp, L., Bousquet, P., et al.: Two decades of ocean CO_2 sink and variability, Tellus, Ser. B, 55, 649–656, 2003.
Mahowald, N. M., Rasch, P. J., Eaton, B. E., Whittlestone, S., and Prinn, R. G.: Transport of radon-222 to the remote troposphere using the Model of Atmospheric Transport and Chemistry and assimilated winds from ECMWF and the National Center for Environmental Prediction/NCAR, J. Geophys. Res., 102, 28 139–28 151, 1997.
Manning, A. C. and Keeling, R. F.: Global oceanic and land biotic carbon sinks from the Scripps atmospheric oxygen flask sampling network, Tellus B, 58, 95–116, 2006.
Marland, G., Boden, T. A., and Andres, R. J.: Global, regional, and national CO_2 emissions, in Trends: A Compendium of Data on Global Change, pp. 505–584, Carbon Dioxide Inf. Anal. Cent., Oak Ridge Natl. Lab., U.S. Dep. of Energy, Oak Ridge, Tenn., available at http://cdiac.esd.ornl.gov/trends/emis/tre_glob.htm, 2003.
Matsumoto, K., and Gruber, N.: How accurate is the estimation of anthropogenic carbon in the ocean? An evaluation of the ΔC^* method, Global Biogeochem. Cycles, 19, GB3014, doi:10.1029/2004GB002397, 2005.
McKinley, G. A., Follows, M. J., Marshall, J., and Fan, S. M.: Interannual variability of air-sea O_2 fluxes and the determination of CO_2 sinks using atmospheric O_2/N_2, Geophys. Res. Lett., 30, 1101, doi:10.1029/2002GL016044, 2003.
Moore, J. K., Doney, S. C., Kleypas, J. C., Glover, D. M., and Fung, I. Y.: An intermediate complexity marine ecosystem model for the global domain, Deep-Sea Res. Pt. II, 49, 403–462, 2002.
Moore, J. K., Doney, S. C., and Lindsay, K.: Upper ocean ecosystem dynamics and iron

cycling in a global three-dimensional model, Global Biogeochem. Cycles, 18, GB4028, doi:10.1029/2004GB002220, 2004.
Naegler, T., Ciais, P., Orr, J. C., Aumont, O., and Roedenbeck, C.: On evaluating ocean models with atmospheric potential oxygen, Tellus, 59B, 138–156, 2007.
Najjar, R. G. and Keeling, R. F: Mean annual cycle of the air-sea oxygen flux: A global view, Global Biogeochem. Cycles, 14(2), 573–584, 2000.
Nevison, C. D., Keeling, R. F., Weiss, R. F., Popp, B. N., Jin, X., Fraser, P. J., Porter, L. W., and Hess, P. G.: Southern Ocean ventilation inferred from seasonal cycles of atmospheric N_2O and O_2/N_2 at Cape Grim, Tasmania, Tellus, 57B, 218–229, 2005.
Olsen, S. C. and Randerson, J. T.: Differences between surface and column atmospheric CO_2 and implications for carbon cycle research, J. Geophys. Res., 109, D02301, doi:10.1029/2003JD003968, 2004.
Plattner, G. K., Joos, F., and Stocker, T. F.: Revision of the global carbon budget due to changing air-sea oxygen fluxes, Global Biogeochem. Cycles, 16, GB1096, doi:10.1029/2001GB001746, 2002.
Prentice, I. C., Farquhar, G. D., Fasham, M. J. R., Goulden, M. L., Heimann, M., Jaramillo, V. J., Kheshgi, H. S., and Le Quéré, C.: The carbon cycle and atmospheric carbon dioxide, in Climate Change 2001: The Scientific Basis, Contribution of Working Group I to the Third Assessment Report of the Intergovernmental Panel on Climate Change, edited by J. T. Houghton et al., pp. 183–287, Cambridge Univ. Press, New York, 2001.
Randerson, J. T., van der Werf, G. R., Collatz, G. J., Giglio, L., Still, C. J., Kasibhatla, P., Miller, J. B., White, J. W. C., DeFries, R. S., and Kasischke, E. S.: Fire emissions from C3 and C4 vegetation and their influence on interannual variability of atmospheric CO_2 and $\delta^{13}CO_2$, Global Biogeochem. Cycles, 19, GB2019, doi:10.1029/2004GB002366, 2005.
Rasch, P. J., Mahowald, N. M., and Eaton, B. E.: Representations of transport, convection, and the hydrologic cycle in chemical transport models: Implications for the modeling of short-lived and soluble species, J. Geophys. Res., 102, 28 127–28 138, 1997.
Sarmiento, J. L., Hughes, T. M. C., Stouffer, R. J., and Manabe, S.: Simulated response of the ocean carbon cycle to anthropogenic climate warming, Nature, 393, 245–249, 1998.
Severinghaus, J. P.: Studies of the terrestrial O_2 and carbon cycles in sand dune gases and in Biosphere 2, Ph.D. thesis, Columbia University, New York, 1995.
Stephens, B. B., Keeling, R. F., Heimann, M., Six, K. D., Murnane, R., and Caldeira, K.: Testing global ocean carbon cycle models using measurements of atmospheric O_2 and CO_2

concentration, Global Biogeochem. Cycles, 12, 213–230, 1998.
Takahashi, T., Poisson, A. Metzl, N., Tilbrook, B., Bates, N., and coauthors: Global sea-air CO_2 flux based on climatological surface ocean pCO_2, and seasonal biological and temperature effects, Deep-Sea Res. Pt. II, 49, 1601–1622, 2002.
Taylor, K. E.: Summarizing multiple aspects of model performance in a single diagram, J. Geophys. Res., 106, 7183–7192, 2001.
Thoning, K. W., Tans, P. P., and Komhyr, W. D., Atmospheric carbon dioxide at Mauna Loa Observatory: 2. Analysis of the NOAA GMCC data, 1974–1985, J. Geophys. Res., 94, 8549–8565, 1989.
Van der Werf, G. R., Randerson, J. T., Giglio, L., Collatz, G. J., Kasibhatla, P. S., and Arellano Jr., A. F.: Interannual variability in global biomass burning emissions from 1997 to 2004, Atmos. Chem. Phys., 6, 3423–3441, 2006, http://www.atmos-chem-phys.net/6/3423/2006/.

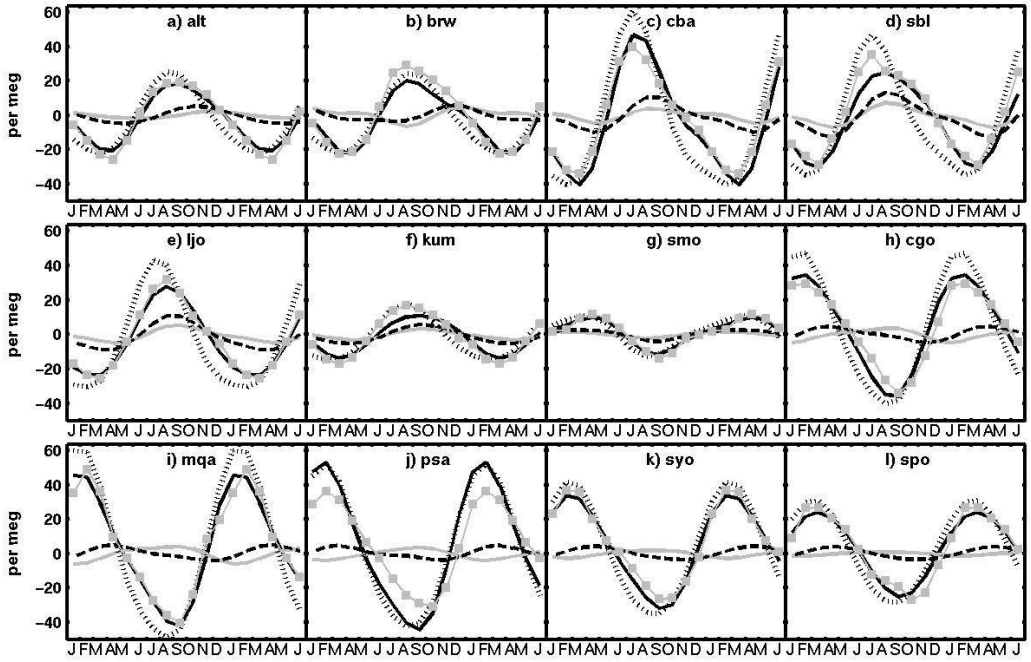

Fig. 1. Seasonal cycles of APO^{oc} at 12 selected stations. Gray filled squares are fit to the Battle et al. (2006) observed climatological seasonal cycle; black solid line is WHOI/MATCH APO^{oc}; black dotted line is the seasonal climatology/MATCH APO^{oc} (GK01/Takahashi et al., 2002) ; gray solid line is WHOI/MATCH CO_2^{oc}, in per meg units; black dashed line is APO^{oc} calculated with WHOI thermal O_2 rather than total O_2^{oc}. Seasonal cycles were calculated by detrending the MATCH results with a 3rd order polynomial + 4 harmonics fit (Thoning et al., 1989; Nevison et al., 2007) and subtracting the annual mean. **(a)** Alert, Canada (ALT), **(b)** Barrow, Alaska (BRW), **(c)** Cold Bay, Alaska (CBA), **(d)** Sable Island, Nova Scotia (SBL), **(e)** La Jolla, CA (LJO), **(f)** Kumukahi, Hawaii (KUM), **(g)** Samoa (SMO), **(h)** Cape Grim, Tasmania (CGO), **(i)** MacQuarie Island, Australia (MQA), **(j)** Palmer Station, Antarctica (PSA), **(k)** Syowa, Antarctica (SYO), **(l)** South Pole (SPO).

BGD
4, 2877–2914, 2007

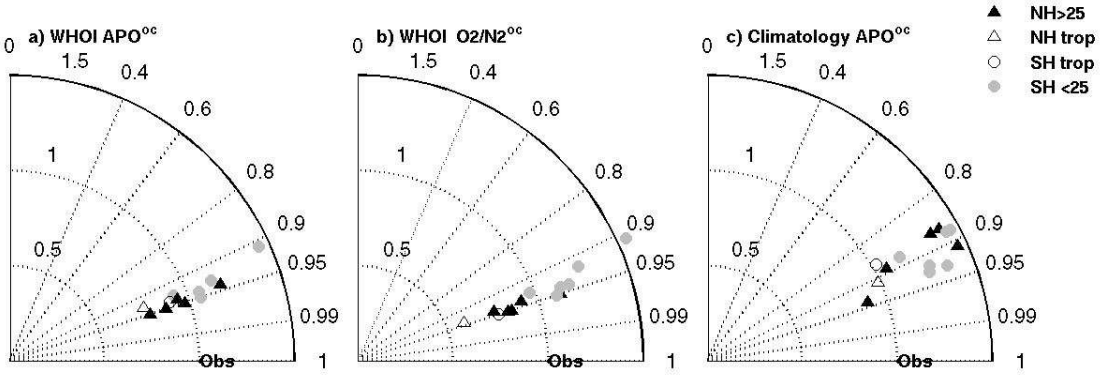

Fig. 2. Taylor diagrams summarizing the comparison of MATCH seasonal cycles to Battle et al. (2006) observations. The angle θ from the x-axis in the polar plot is the arccosine of the correlation coefficient R between the model and observed cycle, which reflects the agreement in shape and phasing. The value on the radial axis is the ratio of standard deviations: $\sigma_{\text{model}}/\sigma_{\text{obs}}$, which represents the match between the amplitude of the model and observed seasonal cycle (Taylor, 2001). Each symbol represents 1 of the 12 stations in Fig. 1, or a 13th station, Amsterdam Island, France (AMS). The 13 stations are sorted into 4 latitude bands according to the figure legend. **(a)** WHOI/MATCH APO^{oc}, **(b)** WHOI/MATCH O_2/N_2^{oc} (CO_2^{oc} not included), **(c)** seasonal climatology/MATCH APO^{oc}.

BGD
4, 2877–2914, 2007

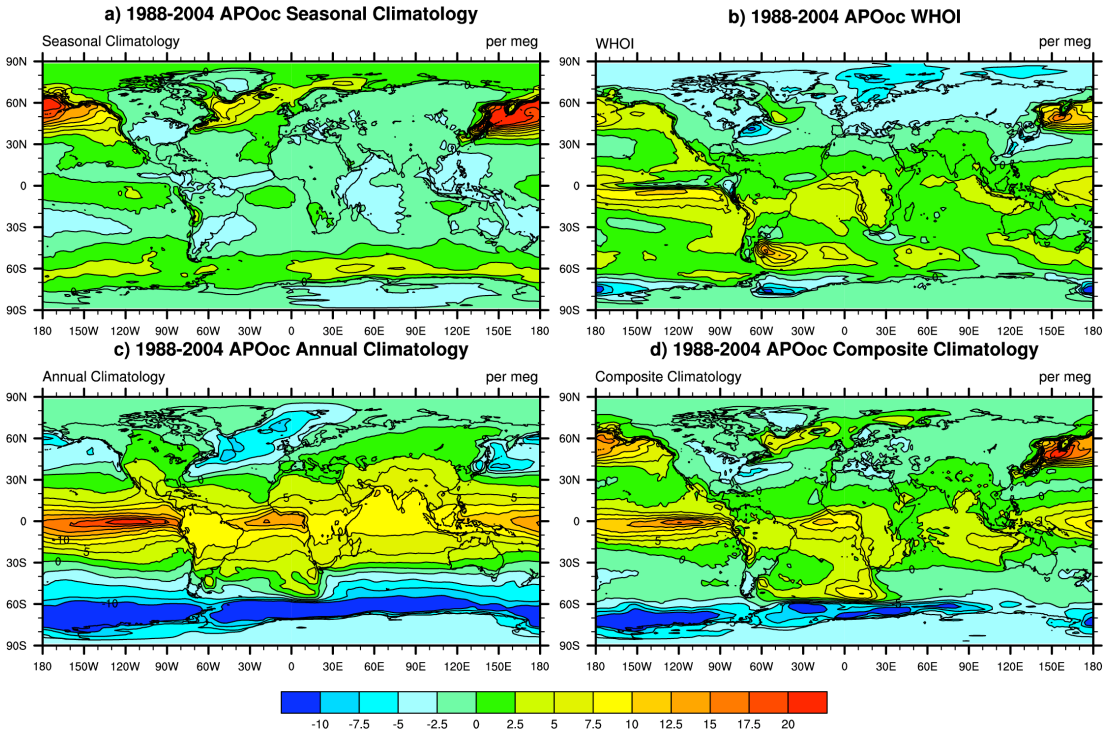

Fig. 3. First column: The annual mean seasonal rectifier in APO^{oc}, calculated by averaging detrended MATCH tracers from 1988–2004 and subtracting the global mean: $APO^{oc} = \frac{1}{XO2}(O_2^{oc} - meanO_2^{oc}) - \frac{1}{XN2}(N_2^{oc} - meanN_2^{oc}) + \frac{1.1}{XO2}(CO_2^{oc} - meanCO_2^{oc})$ **(a)** seasonal climatology, **(b)** WHOI, **(c)** annual climatology, including annual O_2 and N_2 fluxes (Gruber et al., 2001; Gloor et al., 2001) with Takahashi et al. (2002) CO_2^{oc}, **(d)** composite seasonal/annual climatology computed as the sum of (a) and (c) (Note: Takahashi et al. ([redacted]**year?**) CO_2^{oc} is used in both the seasonal and annual climatology, but is counted just once in the composite climatology).

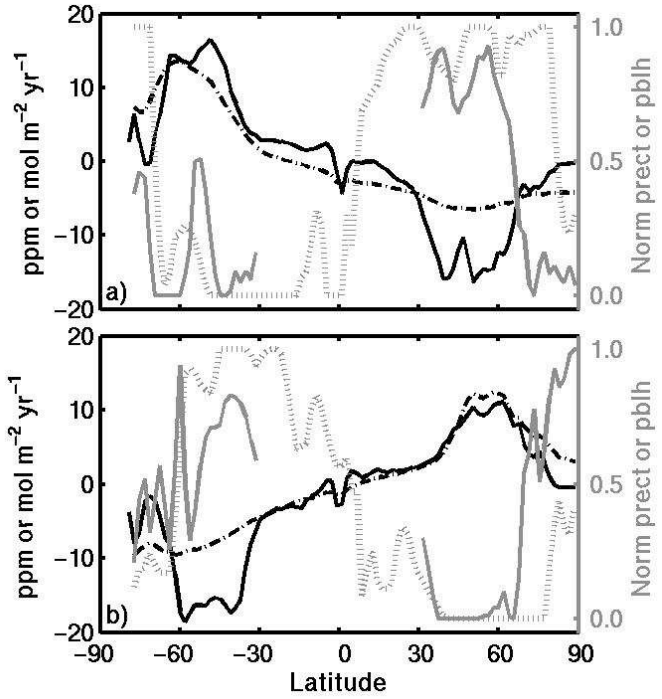

Fig. 4. Zonal averages (over ocean regions only) exploring the cause of the seasonal rectifier effect for **(a)** January, **(b)** July. Black solid line is the WHOI oceanic O_2 flux (mol m^{-2} yr^{-1}); black dot-dash line is the WHOI/MATCH O_2 seasonal anomaly (ppmv); gray dotted line is the MATCH planetary boundary layer height (pblh); gray solid line is the sum of MATCH large scale and convective precipitation (prect), a proxy for ventilation of surface layers by upward motion associated with storms. Both pblh and prect are normalized at each latitude band according to the annual mean value in that band. Prect is masked equatorward of 30° because convective precipitation has strong patterns there that distract from the mid-latitude patterns the figure seeks to emphasize.

BGD
4, 2877–2914, 2007

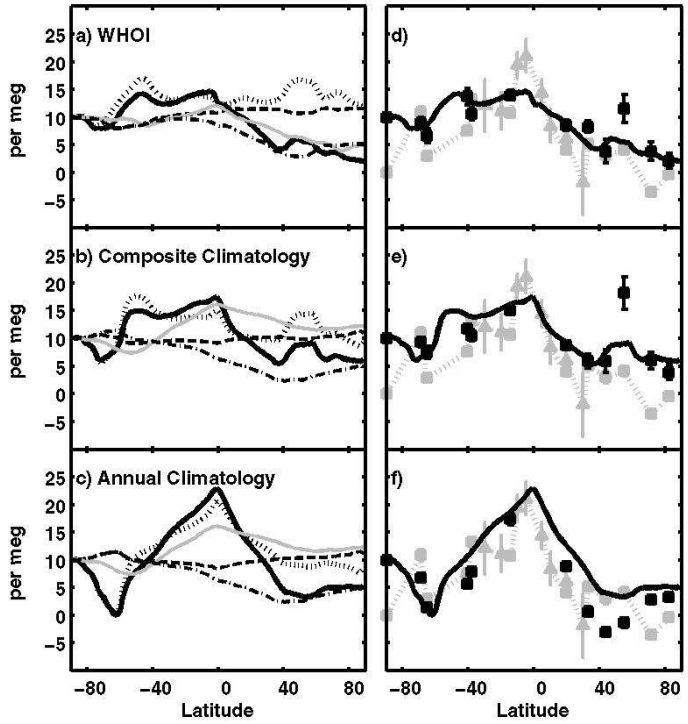

Fig. 5. Top row: Components of MATCH zonally averaged annual mean APO, in which all values are normalized to the South Pole and expressed in per meg units. Black heavy line is total APO, including fossil fuel; dotted line is oceanic O_2; dashed line is oceanic N_2; solid gray line is oceanic CO_2; dash-dot line is fossil fuel. **(a)** WHOI, **(b)** composite (seasonal+annual) climatology, **(c)** annual climatology. Bottom row compares MATCH annual mean latitudinal gradient in APO to Battle et al. (2006) station (gray squares) and shipboard (gray triangles) data. Black squares are MATCH annual mean values at the Battle et al. (2006) stations, which differ in some cases from the zonal averages. Since the values at the SPO are arbitrary, all results have been shifted to aid visual comparison.

BGD
4, 2877–2914, 2007

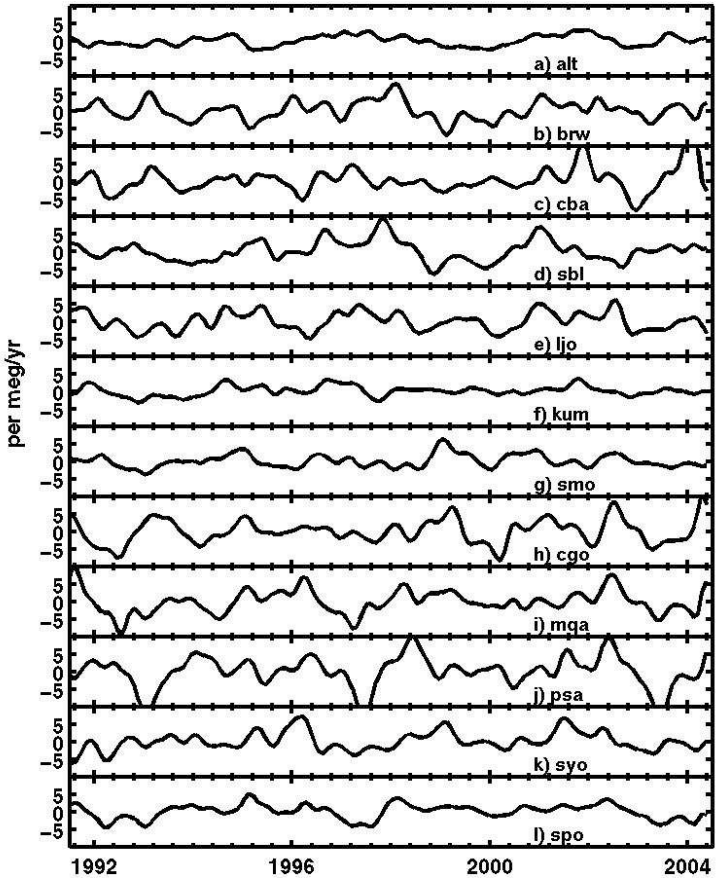

Fig. 6. Interannual variability in WHOI/MATCH APO calculated by using Eq. (1), removing the seasonal cycle with a 12-month running average and taking the slope of the deseasonalized time series as a central difference. Stations a) to l) as in Fig. 1.

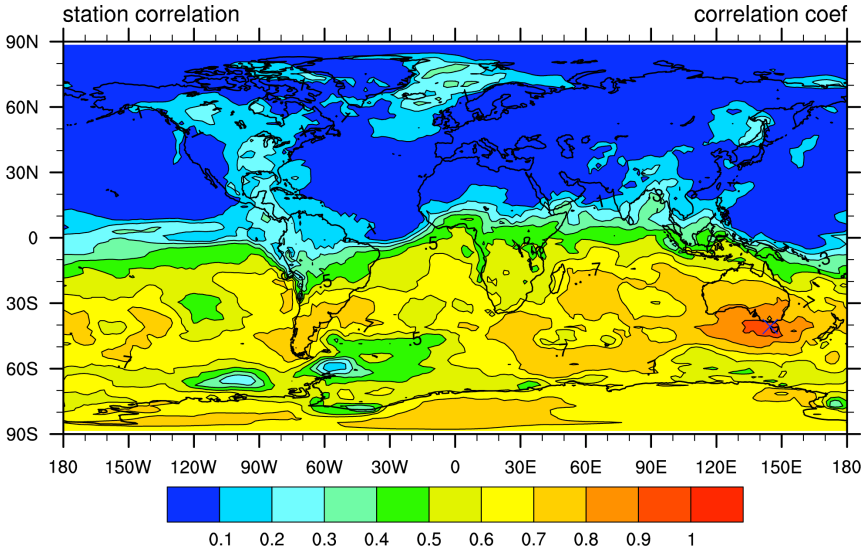

Fig. 7. Spatial coherence of interannual variability in WHOI/MATCH APO. Shows the correlation coefficient R between the Cape Grim, Tasmania station and all other gridpoints in the 1988-2004 deseasonalized MATCH APO time series. Station location is indicated by a blue X. Similar patterns are seen for the other stations in Fig. 1.

BGD
4, 2877–2914, 2007

EGU

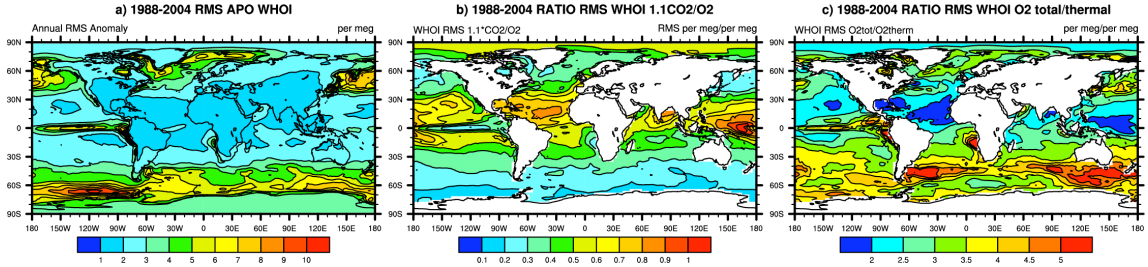

Fig. 8. **(a)** Interannual RMS variability 1988–2004 in WHOI/MATCH APO^{oc} computed as the RMS of the differences between each month and the corresponding month from the MATCH climatological seasonal cycle (e.g., model January 1998 minus model climatological January). **(b)** Ratio of RMS variablities $1.1CO_2^{oc}$:O_2^{oc}. **(c)** Ratio of RMS variablities O_2^{oc}:$O_2^{thermal}$.

BGD
4, 2877–2914, 2007

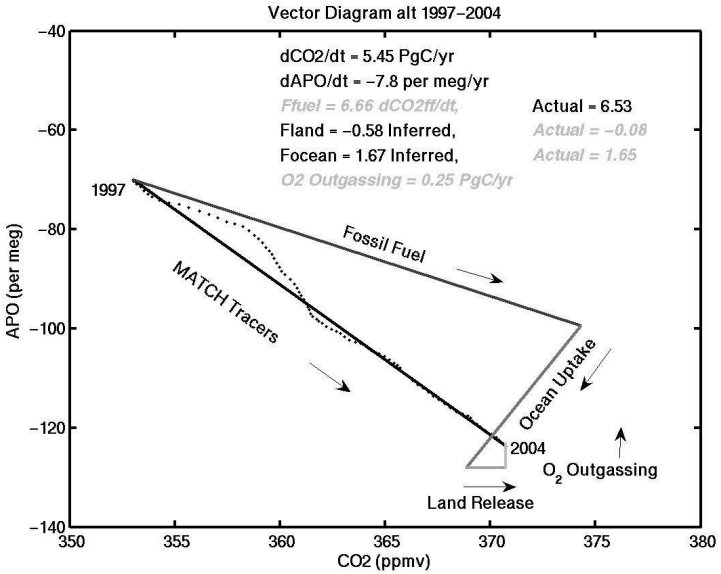

Fig. 9. Vector diagram showing ΔAPO/Δt and $\Delta CO_2/\Delta t$ from 1997 to 2004 for WHOI/MATCH APO sampled at station Alert. The carbon sinks F_{land} and F_{ocean} inferred by solving Eqs. (5) and (3) are compared to the "actual" surface fluxes used to force the MATCH simulation. The time derivative of the MATCH fossil fuel tracer $\Delta CO_2^{FF}/\Delta t$ is also compared to the actual F_{fuel} used to force MATCH. The O_2 outgassing term (Z_{eff}) is computed as $Z_{eff}=[\frac{1}{XO2}(fO_2^{oc})-\frac{1}{XN2}(fN_2^{oc})]/M*10^6/(\beta\gamma\alpha_{bio})p$, where fO_2^{oc} and fN_2^{oc} are the globally integrated WHOI ocean fluxes in moles/yr used to force MATCH, $M=1.768\times10^{20}$ is the total moles of dry air in the atmosphere, and β, γ and α_{bio} are conversion factors defined in the text that convert per meg to Pg C. Gray italic text denotes quantities known in the model simulation but unknown in the real world. Unless labeled otherwise, all these quantities are in PgC/yr, averaged over the 8 year interval 1997–2004. Note that F_{land} in the model is actually a small source of carbon and thus has a negative value in the diagram, since F_{land} and F_{ocean} are defined as positive when they act as sinks.

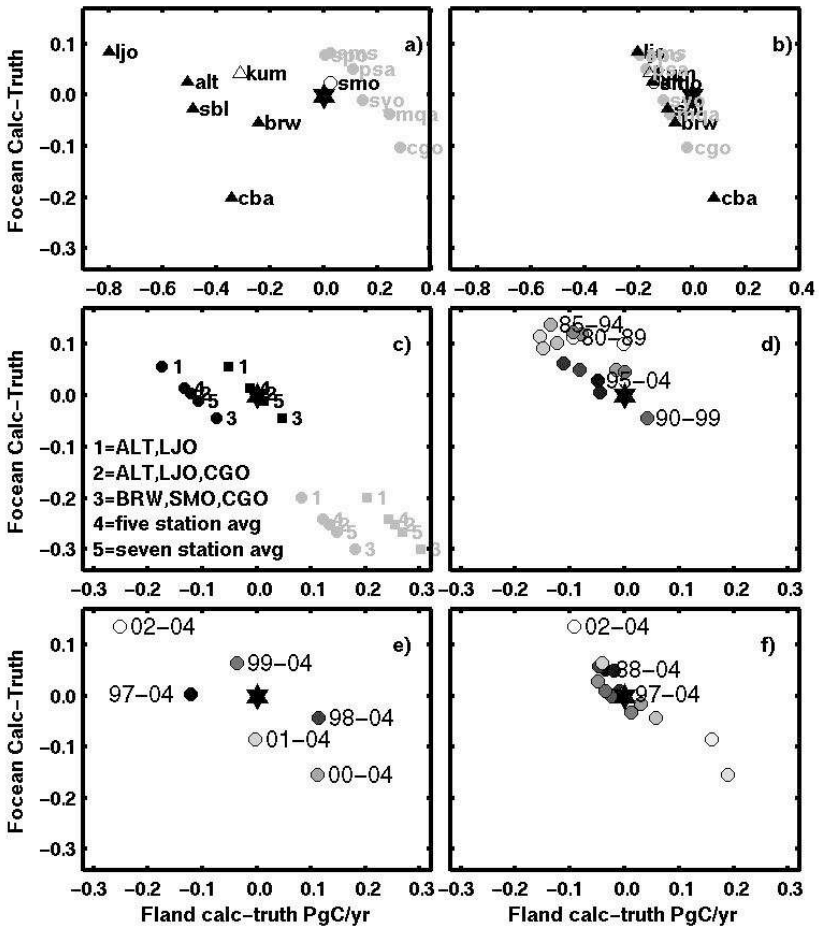

Fig. 10.

BGD
4, 2877–2914, 2007

EGU

Fig. 10. Summary of calculations solving Eqs. (4) and (2) for F_{land} and F_{ocean} using WHOI/MATCH tracers. The difference between inferred and actual F_{land} and F_{ocean} is shown on the x and y-axis, respectively, in Pg C/yr. The "truth" at x=0, y=0 is marked with a star. **(a)** 1997–2004 using GFED land CO_2 tracer. $\Delta APO/\Delta t$ and $\Delta CO_2/\Delta t$ are evaluated separately at 13 individual stations, as labeled on plot, using legend symbols described in Fig. 2. **(b)** same as (a) except using global $\Delta CO_2/\Delta t$. **(c)** 1997–2004 using GFED (circles) or NB (squares) land CO_2 tracer. The numbers 1-5 indicate the combination of stations used to calculate average $\Delta APO/\Delta t$: 1=ALT, LJO, 2=ALT, LJO, CGO, 3=BRW, SMO, CGO, 4=ALT, LJO, KUM, CGO, PSA, 5=ALT, CBA, LJO, KUM, SMO, CGO, PSA. Global $\Delta CO_2/\Delta t$ is used for all cases. Gray symbols are corresponding solutions when the O_2 outgassing correction is omitted. Panels d-f all use the ALT, LJO, CGO station average for $\Delta APO/\Delta t$ and global $\Delta CO_2/\Delta t$. **(d)** Shows 17 staggered 10-year intervals, using NB land, from 1979–1988 (lightest circle) to 1995–2004 (darkest). The 4 intervals featured in Fig. 11 are explicitly labeled. **(e)** Shows 6 varied time intervals using GFED land CO_2, from 1997–2004 (darkest) to 2002–2004 (lightest). **(f)** Shows 24 varied time intervals using NB land CO_2 from 1988–2004 (darkest) to 2002–2004 (lightest).

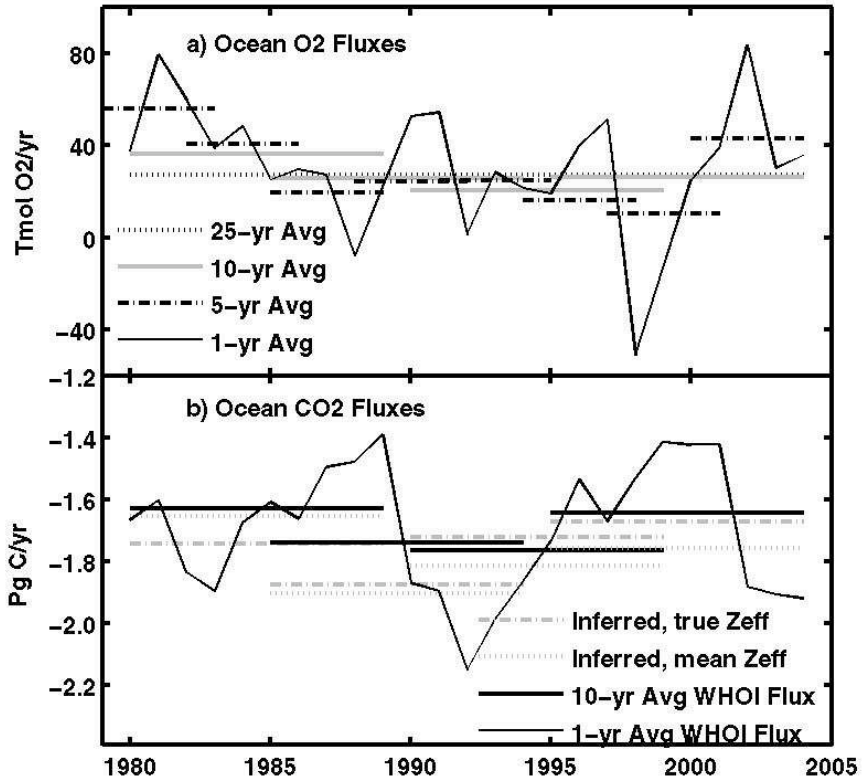

Fig. 11. **(a)** Globally integrated WHOI sea-to-air O_2 flux (in Tmol O_2/yr) shown as 1-yr (thin black line), 5-yr (dot-dash lines), 10-yr (gray solid line) and 25-yr (dotted line) averages. **(b)** Globally integrated WHOI sea-to-air CO_2 flux (in Pg C/yr) shown as 1-yr (thin black line) and 10-yr (heavy black line) averages. Gray lines show inferred F_{ocean} from calculation described in 10d) solved for 4 different 10-yr intervals, using true Z_{eff} (dash-dot) and 25-yr average Z_{eff} (dotted).

BGD
4, 2877–2914, 2007

EGU

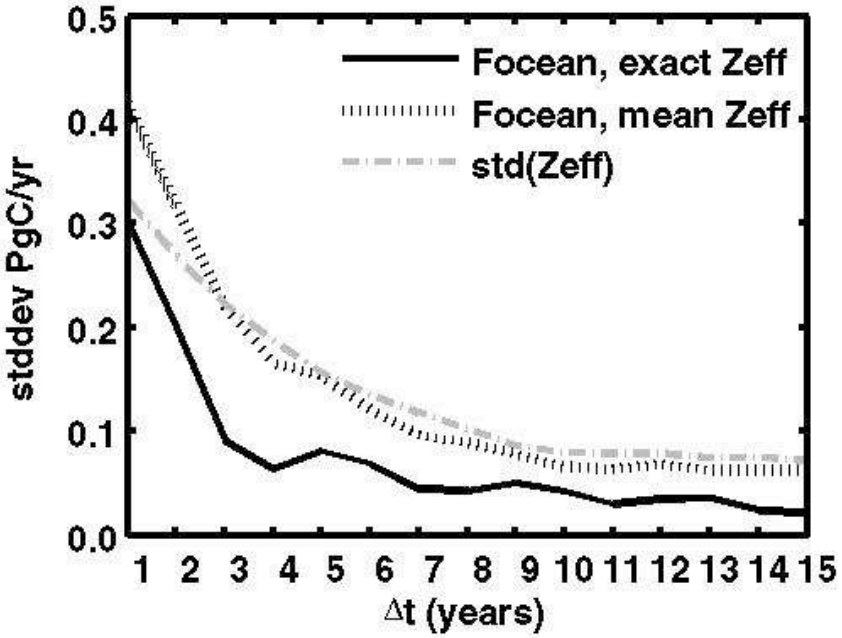

Fig. 12. Summary of standard deviations in inferred minus true F_{ocean} (in Pg C/yr). Calculations use deseasonalized WHOI/MATCH results over Δt intervals ranging from 1 to 15 years, in which all whole-year staggered intervals for each respective Δt between 1980 and 2003 are considered (e.g., N=24 intervals for Δt=1 and N=10 intervals for Δt =15). Black solid line shows results using true Z_{eff} over the interval Δt; black dotted line shows results using the 1980–2003 mean Z_{eff}; Gray dot-dash line shows the standard deviation of mean minus true Z_{eff} (converted to PgC/yr as described in Fig. 9) for the N staggered intervals at each Δt. All calculations use global $\Delta CO_2/\Delta t$, the ALT, LJO, CGO station average for ΔAPO/Δt, and the NB land CO_2 tracer.

BGD
4, 2877–2914, 2007